Solid Earth

Hydroxyl in eclogitic garnet, orthopyroxene, and oriented inclusion-bearing clinopyroxene, western Norway

Dirk Spengler[1]**, Monika Koch-Müller**[2]**, Adam Włodek**[1]**, Simon J. Cuthbert**[1]**, and Jarosław Majka**[1,3]

[1]Department of Mineralogy, Petrography and Geochemistry, AGH University of Krakow,
al. A. Mickiewicza 30, 30-059 Krakow, Poland
[2]Deutsches GeoForschungsZentrum GFZ, Telegrafenberg, 14473 Potsdam, Germany
[3]Department of Earth Sciences, Uppsala University, Villavägen 16, 752-36 Uppsala, Sweden

Correspondence: Dirk Spengler (dirk@spengler.eu)

Abstract. A total of 10 western Norwegian eclogites, whose mineral chemistry records metamorphism of up to 850 °C and 5.5 GPa, were investigated for structural hydroxyl content in nominally anhydrous minerals. Garnet shows pronounced absorption in the wavenumber ranges of 3596–3633, 3651–3694, and 3698–3735 cm^{-1} and minor absorption centred at about 3560 cm^{-1}. Clinopyroxene with aligned inclusions of either quartz, albite, or quartz + pargasite has major absorption at 3450–3471 and 3521–3538 cm^{-1} and minor absorption centred at 3350 and approximately 3625 cm^{-1}. The latter band is strongest in a sample with minute lamellar inclusions rich in Al, Fe, and Na and was excluded from hydroxyl quantification. Orthopyroxene has large, narrow absorption peaks centred at 3415 and 3515 cm^{-1} and smaller peaks at 3555, 3595, and 3625 cm^{-1}. Five orthopyroxene-bearing eclogites exhibit relatively homogeneous amounts of structural hydroxyl in garnet (13–32 $\mu g\, g^{-1}$), clinopyroxene (119–174 $\mu g\, g^{-1}$), and orthopyroxene (4–17 $\mu g\, g^{-1}$). The outer 200 μm wide rims of the orthopyroxene grains illustrate a late hydroxyl loss compared to core values of about 30 %, which is not evident in garnet and clinopyroxene. In contrast, the other five orthopyroxene-free eclogites exhibit variable amounts of hydroxyl in garnet (8–306 $\mu g\, g^{-1}$) and clinopyroxene (58–711 $\mu g\, g^{-1}$). Apart from extreme values, the structural hydroxyl content of clinopyroxene in the eclogites studied is lower than in comparable ultra-high-pressure metamorphic samples, e.g. both metasomatised and pristine eclogite xenoliths from the lithospheric mantle underneath several cratons and coesite- and quartz-eclogites from the Erzgebirge and the Kokchetav mas-

sifs, by up to several hundreds of micrograms per gram ($\mu g\, g^{-1}$). The low structural hydroxyl contents, the deficiency of molecular water, and the preservation of diffusion-sensitive evidence from the mineral chemistry for metamorphism well beyond the stability field of amphibole suggest that oriented inclusions of quartz + pargasite were formed isochemically during decompression. In addition, structural hydroxyl content in clinopyroxene is inversely correlated with metamorphic pressure estimates obtained from orthopyroxene of the same samples. Therefore, structural hydroxyl in nominally anhydrous eclogite minerals can serve as an indicator of the effectiveness of retrogression.

1 Introduction

Nominally anhydrous minerals (NAMs) in eclogite contain crystallographically bound hydroxyl, which is an important information carrier during the evolution of the rock at high-grade metamorphism and subsequent retrogression (Gose and Schmädicke, 2018, 2022). For example, the structural hydroxyl can indicate whether eclogite-facies hydrous minerals were once present, whether fluid inflow occurred, and whether decompression was accompanied by dehydroxylation. At the same time, mineral chemistry, textures, and inclusion microstructures are known to also carry important information, for example, by partitioning temperature- and pressure-sensitive elements between coexisting minerals (i.e. geothermometers and geobarometers) or by the breakdown of unstable components from solid solutions,

forming symplectic reaction textures (as in the decomposition of the jadeite component in omphacite; Anderson and Moecher, 2007) or oriented quartz inclusions (Ca-Eskola; Smith, 1984). From experimental and theoretical petrology, it is known that a change in mineral chemistry and/or the formation of a reaction texture or inclusion microstructure can be explained by different, sometimes contradictory, processes. However, when these features occur together in natural samples, the processes underlying them must be consistent with the geodynamic environment of the evolution of the rocks. This reduction in ambiguity is particularly beneficial for understanding the formation of oriented, notably structural hydroxyl-bearing mineral inclusions in NAMs.

Experimental work has shown that the stability field of the Ca-Eskola component ($Ca_{0.5}\square_{0.5}AlSi_2O_6$) in clinopyroxene is almost entirely beyond that of quartz (Konzett et al., 2008a). This suggests that oriented quartz needles in natural clinopyroxene from a variety of ultra-high-pressure (UHP) metamorphic areas formed by isochemical exsolution during decompression (Smith, 1984; Shatsky et al., 1985; Bakun-Czubarow, 1992; Katayama et al., 2000; Schmädicke and Müller, 2000; Dobrzhinetskaya et al., 2002; Song et al., 2003; Janák et al., 2004, 2013; Zhang et al., 2005). Some natural occurrences have such quartz needles in close spatial association with amphibole needles, which also, by analogy, were proposed to have been exsolved from a former UHP clinopyroxene (Terry et al., 2000). However, the mineral minor and trace element chemistry and the inclusion distribution provide arguments for an alternative origin of the bimineralic oriented inclusions. They were suggested to have formed either by alteration and precipitation in an open system through chemical exchange with fluids or associated minerals (Proyer et al., 2009; Liu and Massonne, 2022) or alternatively during progressive growth of the host mineral long before retrogression (Konzett et al., 2008b). By implication, the bimineralic oriented inclusions in clinopyroxene would not constitute evidence for a former Ca-Eskola component and thus formerly UHP metamorphic conditions.

The aim of this study is to determine the origin and thus the significance of lamellar amphibole occurring in close spatial association with lamellar quartz in clinopyroxene in eclogites of the Western Gneiss Region (WGR) in Norway. For this purpose, we quantified the structural hydroxyl content in NAMs of 10 previously studied eclogites (Fig. 1; the abbreviations of mineral phases in figures, captions, and the table follow the nomenclature of Warr, 2021). What the eclogites have in common is that they contain clinopyroxene with aligned inclusions of either quartz, albite, or quartz + pargasite, which are thought to have formed following UHP metamorphism, while the current mineral chemistry suggests variable metamorphic conditions between 700–850 °C and 2.1–5.5 GPa for most of the samples (Spengler et al., 2023). In addition, we analysed the spatial distribution of major elements in clinopyroxene in 1 of the 10 samples. The mineral hydroxyl content is placed in context with petrological information to evaluate possible origins for the amphibole lamellae-bearing (bimineralic) and amphibole lamellae-free (monomineralic) oriented inclusion microstructures. We will show that the hydroxyl content of NAMs is low and independent of the lamellar type present in the sample but is high when hydrous minerals are present in the eclogite facies or when strong retrograde overprinting occurred.

2 Geological setting and sample description

The Scandinavian Caledonides were formed during the closure of the Iapetus Ocean in the early Paleozoic and the subsequent collision of the continents Laurentia and Baltica (Gee et al., 2013). This collision caused the thrusting of nappes with peripheral, outboard, and Laurentian affinities onto the Baltica plate margin, where they formed an east-verging tectonostratigraphic succession (Gee et al., 1985). The WGR constitutes a tectonic window through this nappe pile onto the lowermost tectonostratigraphic unit, the Lower Allochthon, which exposes high-grade metamorphic rocks with Proterozoic protolith ages (Kullerud et al., 1986; Tucker et al., 1990). These Proterozoic Baltica basement gneisses, together with minor infolded supracrustal rocks (Krill, 1980), were reworked during the Caledonian orogeny. Radiogenic ages from high-grade quartzo-feldspathic gneiss and enclosed lenses of deformed mafic and ultramafic rocks (eclogite and pyroxenite) in the WGR suggest that maximum UHP metamorphic conditions during plate convergence in this area occurred during the final Silurian to early Devonian ("Scandian") phase of the orogeny (Griffin and Brueckner, 1980; Carswell et al., 2003; Tucker et al., 2004; Spengler et al., 2009; Walczak et al., 2019).

Direct evidence for UHP metamorphism of gneiss is limited to a few occurrences along the coast in the form of polycrystalline inclusions of quartz (inferred to be after coesite) in clinopyroxene, zoisite, and clinozoisite (Wain et al., 2000); inclusions of coesite in detrital garnet (Schönig et al., 2018); and grains of diamond recovered from a crushed and dissolved sample (Dobrzhinetskaya et al., 1995). Evidence for UHP metamorphism of mafic and ultramafic rocks, exposed as isolated lenses within gneiss, is also concentrated along the coast in terms of index mineral inclusions, i.e. coesite in eclogitic clinopyroxene, garnet, and zircon (Smith, 1984; Wain, 1997; Carswell et al., 2003; Root et al., 2005); diamond in eclogitic zircon (Smith and Godard, 2013); and diamond in pyroxenitic Cr-spinel and garnet (van Roermund et al., 2002; Vrijmoed et al., 2006). Furthermore, these mafic and ultramafic rocks provide evidence that UHP metamorphism extended spatially from the coast to the landward end of some fjords. Among them are polycrystalline inclusions of quartz in clinopyroxene and garnet from eclogite (Smith, 1984; Cuthbert et al., 2000; Walsh and Hacker, 2004) and oriented monomineralic inclusions of quartz in
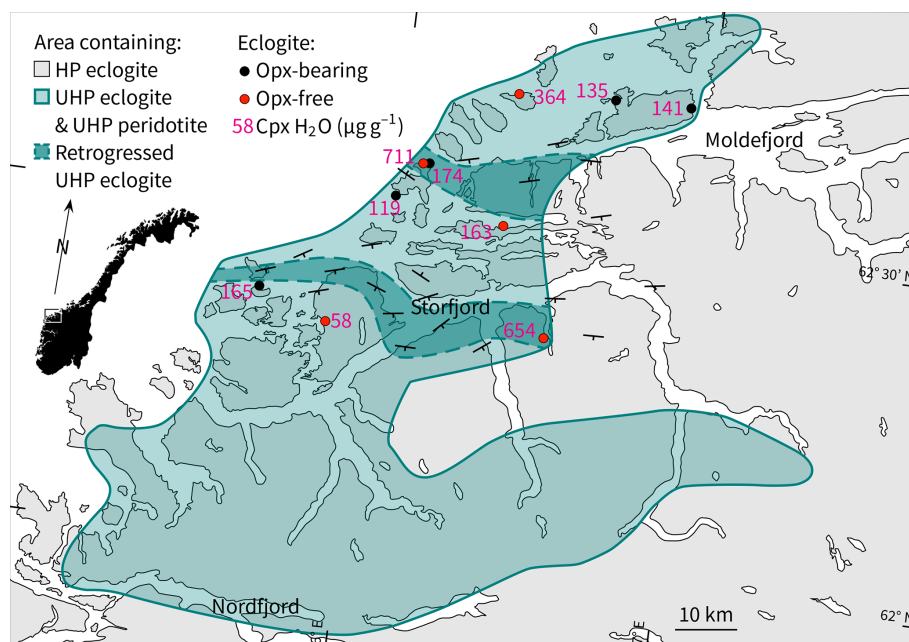
Figure 1. Simplified map of the WGR that shows an area with evidence for UHP metamorphism from eclogite (Smith, 1984; Wain et al., 2000; Root et al., 2005; Spencer et al., 2013; Spengler et al., 2023) and peridotite (Spengler et al., 2009, 2021) enclosed in gneiss using three approaches: index minerals (Coe, Dia), geothermobarometric estimates (exchange equilibria, net-transfer equilibria), and mineral microstructures after precursor mineral phases (polycrystalline Qz inclusions after Coe, oriented Qz inclusions after Ca-Eskola). The dots show locations of samples (this study). Labels refer to structural hydroxyl in Cpx given in Table 1. Samples with elevated structural hydroxyl in Cpx (dependent on whole-rock chemistry) are shown in dark shaded areas, whose dashed outlines were roughly extrapolated using the foliation orientation in gneiss and mylonite shown with strike and dip symbols (Young, 2018).

clinopyroxene (inferred to be after Ca-Eskola) from eclogite (Smith, 1984; Spengler et al., 2023). In addition, classical geothermobarometry of gneiss-hosted pyroxenitic and garnetitic mineral assemblages of pre-Caledonian origin shows that the former residence depth of so-called Mg–Cr-type ultramafites (Carswell et al., 1983) in the subcontinental lithospheric mantle for occurrences near and far from the coast was exclusively in the coesite stability field (Spengler et al., 2009, 2021). Consequently, the tectonic transport medium (gneiss) of the ultramafites should also have been in the stability field of coesite if the model of Brueckner (1998) applies.

The 10 samples analysed for hydroxyl (Table 1) come from outcrops between Storfjord and Moldefjord (9 from islands and 1 from the mainland; Fig. 1) and were previously examined petrographically and mineralogically (Spengler et al., 2023). Of the 10 samples, 5 have the peak metamorphic mineral assemblage garnet + clinopyroxene + orthopyroxene ± rutile ± opaque minerals. These orthopyroxene-bearing eclogites contain clinopyroxene with bimineralic oriented inclusions of quartz + pargasite (Fig. 2a and b). The other 5 samples have the peak metamorphic mineral assemblage garnet + clinopyroxene ± SiO_2 (coesite) ± rutile ± opaque minerals ± kyanite ± apatite. DS1438, which is 1 of these

orthopyroxene-free samples, comes from an outcrop that is reported to contain minor hydrous minerals as part of the peak UHP metamorphic mineral assemblage (zoisite and phengite in sample 1066b of Terry et al., 2000; phengite in sample FJ-3C of Liu and Massonne, 2022) but which could not be identified in the thin sections prepared. Since the outcrop size is only 5 m × 8 m, we assume that sample DS1438 was in equilibrium with hydrous minerals during peak metamorphism. The investigated specimen has clinopyroxene-hosted bimineralic oriented inclusions of quartz + pargasite as described earlier (Terry et al., 2000). The other 4 orthopyroxene-free eclogites contrast with oriented inclusions of quartz, quartz + albite, or albite, i.e. without pargasite (Fig. 2c and d). Another of these samples (DS2217) has additional, very thin parallel lamellae in clinopyroxene that have not been described previously. Secondary minerals (biotite, amphibole, and plagioclase) occur in the sample suite in varying proportions. Unpublished electron microprobe data of sample DS1438 indicate that the average composition of amphibole occurring in the two different textural positions, i.e. as oriented inclusions in clinopyroxene and as matrix minerals (Fig. S1 in the Supplement), differs by the K_2O content of 0.02 and 0.14 wt %, respectively (Table S1 in the Supplement). The chemistry of

Table 1. FTIR absorption band average peak positions (cm⁻¹) and structural hydroxyl expressed as H_2O equivalent (in µg g⁻¹) of the studied eclogite samples.

Sample, location, P[a]	Eclogite type	Grain area	Cpx (1)	Cpx (2)	Cpx (3)	Cpx (4)	Cpx Grains	Cpx H_2O[b] (1–3)	Cpx H_2O[c] (1–3)	Opx (1)	Opx (2)	Opx (3)	Opx (4)	Opx (5)	Opx (6)	Opx Grains	Opx H_2O[b] (1–6)	Opx H_2O[c] (1–6)	Grt (1)	Grt (2)	Grt (3)	Grt (4)	Grt (5)	Grt (6)	Grt (7)	Grt Grains	Grt H_2O[b] (1–5)	Grt H_2O[b] (1–7)	Grt H_2O[c] (1–5)	Grt H_2O[c] (1–7)
2-4A, Solholmen, 5.17 GPa	Opx-bearing	Rim	3344,	3453,	3537,	3629	4	136	71	3421,	3515,	3546, 3566,	3596	3596	3627	1	8	10	3543,	3603,	3633,	3653,	3693,	3705,	3730	3	28	31	17	20
		core	3344,	3454,	3538,	3626	5	146	78	3418,	3515,	3548, 3565,	3592,	3596,	3628	2	11	13	3553,	3604,	3629,	3651,	3694,	3708,	3732	2	26	28	16	19
		total					6	**141**	75					3611		2	10	13								5	27	29	17	20
DS0326, Remøysunde, 4.05 GPa	Opx-bearing	Rim		3453,	3527,	3621	4	221	124	3541,	3556,	3602,	3654,	3629	3627	2	15	20	3541,	3602,	3632,	3654,		3700,	3730	3	30	38	18	27
		core		3451,	3527,	3626	4	131	73	3531,	3556,	3600,	3651,	3629	3628	2	18	23	3531,	3600,	3630,	3651,		3700,	3730	3	18	26	10	19
		total					4	**165**	92							2	17	21								4	24	32	14	23
DSI409, Syltes, 4.67 GPa	Opx-bearing	Rim	3418,	3463,	3530,	3618	3	119	66	3558,	3597,	3630,	3657,	3675,	3629	4	5	7	3558,	3597,	3630,	3657,	3675,	3698,	3731	4	7	14	4	12
		core		3460,	3530,	3622	3	120	67	3564,	3596,	3627,	3651,		3629	1	7	8	3564,	3596,	3627,	3651,		3698,	3734	3	11	24	6	23
		total					4	**119**	66							2	6	8								4	8	16	5	14
DS2216, Langeneset, 2.20 GPa	Opx-bearing	Rim	3374,	3467,	3525,	3641	4	241	130	3514,	3514,	3558,	3569,	3593,	3626	2	5	7	No reliable data											
		core	3358,	3460,	3521,	3633	4	40	23	3514,	3514,	3558,		3594,	3629	1	8	12	No reliable data											
		total					4	**174**	94							2	6	8												
M65, Korveneset, 4.72 GPa	Opx-bearing	Rim		3450,	3526,	3636	2	162	88	3543,	3604,	3556,	3569,	3596,	3627	2	5	7	3573,	3599,	3630,	3659,	3679,	3700,	3729	3	7	11	4	8
		core	3340,	3453,	3527,	3627	3	114	63	3553,	3553,	3556,		3591,	3616	3	8	10	3568,	3598,	3628,	3655,	3679,	3702,	3730	2	9	16	5	13
		total					3	**135**	74							3	7	9								3	8	13	5	11
DSI438, Fjørtoftvika	Opx-free ±Zo[d]	Rim	3366,	3471,	3527,	3627	5	374	213										3554,	3613,		3653,		3705,	3735	3	285	290	169	175
		core	3338,	3470,			5	358	209										3554,	3613,		3653,			3732	4	309	313	184	189
		total					5	**364**	210																	4	302	306	180	185
DSI405, Riksheim	Opx-free	Rim	3379,	3468,	3523,	3629	5	697	373										3562,	3597,	3631,	3656,		3700,	3731	5	5	10	6	9
		core	3355,	3468,	3524,	3626	6	539	307										3561,	3597,	3629,	3659,		3702,	3730	4	3	8	3	8
		total					6	**654**	355																	4	4	8	5	7
DS2204, Årsøtneset	Opx-free	Rim	3342,	3456,	3530,	3622	3	190	108										3558,	3596,	3629,	3655,	3681,	3699,	3729	3	5	7	3	6
		core	3353,	3454,	3530,	3621	4	136	79										3560,	3597,	3627,	3657,	3693,		3726	1	13	17	6	11
		total					4	**163**	93																	3	8	11	5	8
DS2217, Karmannsvågen	Opx-free	Rim	3385,	3466,	3529,	3621	4	711	384										3558,	3597,	3628,		3686,	3699,	3731	3	12	21	6	16
		core	No reliable data																3563,	3597,	3626,			3699,	3734	4	15	27	8	23
		total					4	**711**	384																	6	13	25	7	20
UL-96-2, Ulsteinvik	Opx-free	Rim	No reliable data	3470,		3622	1	58	31										3561,	3615,	3642,	3650,	3668,	3700,	3732	1	16	18	10	12
		core					1	58	31										3545,	3615,		3656,		3700,	3721	1	16	16	10	10
		total						**58**																			17		10	10

[a] Estimates of metamorphic P are based on Grt–Opx geothermobarometry and were obtained from Spengler et al. (2023). [b] Calibration of Bell et al. (1995). Cpx H_2O contents in bold are those shown in Fig. 1. [c] Calibration of Libowitzky and Rossman (1997). [d] Not identified in the studied thin sections but described in sample 1066 of Terry et al. (2000) taken from the same outcrop.
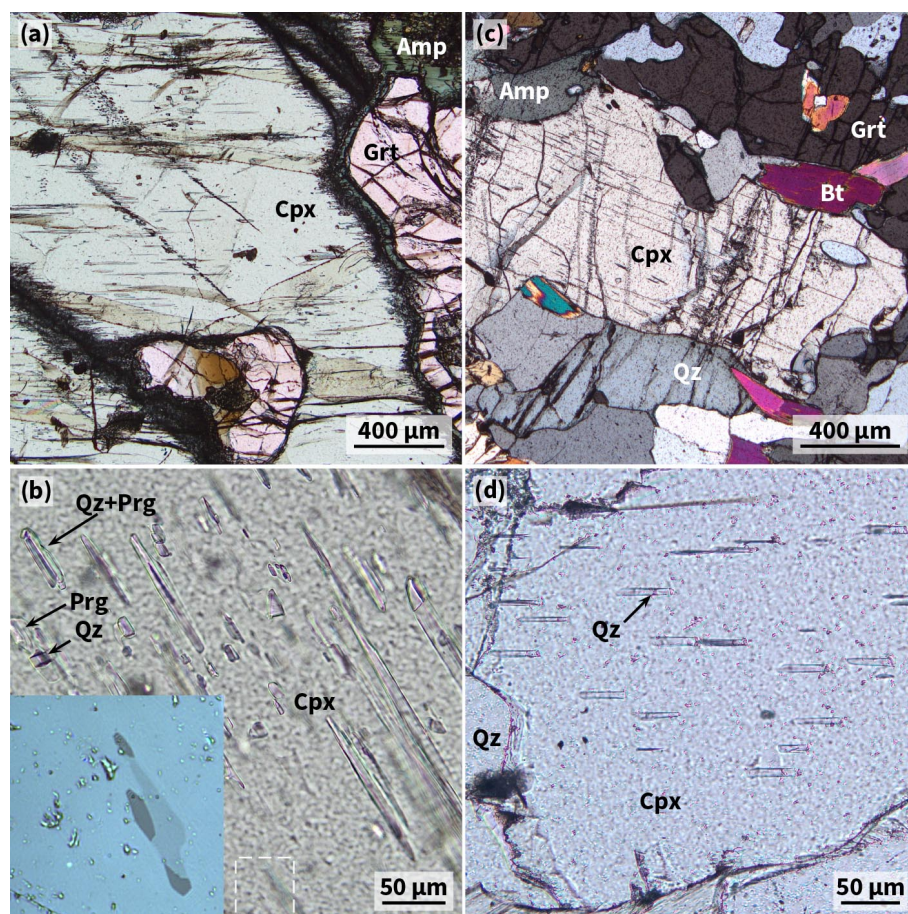
Figure 2. Oriented inclusion-bearing Cpx in WGR eclogite. **(a, b)** Bimineralic needles (plane-polarised light, Synes eclogite DS1409). The dashed frame shows the position of the inset (reflected light). **(c, d)** Monomineralic needles (**c** is nearly cross-polarised light, and **d** is plane-polarised light; Årsetneset eclogite DS2204).

the major and minor elements categorises both amphiboles as pargasite (Locock, 2014).

The orthopyroxene-bearing samples have a pyropic ternary garnet solid solution (with endmember percentages of pyrope 42–58, grossular 9–15, almandine 31–47, and spessartine 1). Orthopyroxene is enstatitic (enstatite 73–86), and clinopyroxene is diopsidic to omphacitic (jadeite + aegirine 6–26). The orthopyroxene-free eclogites have a ternary garnet solid solution with large variation in the almandine content (pyrope 18–50, grossular 21–32, almandine 17–61, and spessartine 0–2). Clinopyroxene is also diopsidic to omphacitic (jadeite + aegirine 6–46) in composition.

3 Methods

Self-supporting double-polished rock slabs were prepared for Fourier transform infrared (FTIR) spectroscopy. The slabs were approximately $20\,mm \times 30\,mm$ in size and 180–$350\,\mu m$ thick. An electronic micrometre caliper was used to measure the slab thickness with a precision of 2–$4\,\mu m$. These slabs were first examined by optical microscopy to locate suitable grains and grain parts that were free of cracks and inclusions or alternatively provided sufficient space in between oriented inclusions for a clear path through the minerals for analysis. Despite this approach, some of the selected sites contain oriented monomineralic inclusions because these could not be avoided. Non-polarised OH absorption spectra were measured using a Bruker VERTEX 80v FTIR spectrometer with an attached Hyperion 2000 microscope at the GFZ. A near-infrared (NIR) light source, a CaF_2 beam splitter, and nitrogen-cooled mercury cadmium telluride (MCT) or InSb detectors were used. Squared apertures with a range in size from $20\,\mu m \times 20\,\mu m$ to $100\,\mu m \times 100\,\mu m$ (dominantly $30\,\mu m \times 30\,\mu m$) were applied to analyse the preselected grain areas. Spectra were taken in the wavenumber range of 4000–$2500\,cm^{-1}$ with a spectral resolution of $2\,cm^{-1}$ and averaged over 256–512 scans. Preferably, several locations inside and at the edge of each grain were analysed,

unless grain geometry, the density of inclusions, or fractures made this impossible.

Absorbance spectra were corrected for interference fringes where appropriate (Neri et al., 1987) and subsequently processed using the open-source software Fityk, version 1.3.2 (Wojdyr, 2010). Each spectrum was baseline-corrected manually using a spline function and deconvolved using a Voigtian function to determine the wavenumber of the peak ν (cm^{-1}) and the area (integral absorbance A_i) of individual absorption bands. The amount of structural hydroxyl was determined from the absorbance of the bands with peak positions in the wavenumber range of 3540–3340 cm^{-1} for clinopyroxene, 3630–3410 cm^{-1} for orthopyroxene, and 3740–3530/3695–3530 cm^{-1} for garnet. Absorption bands > 3600 cm^{-1} for clinopyroxene were attributed to the presence of nanometre-sized inclusions of sheet silicates (group 3 of Koch-Müller et al., 2004) and were not quantified. Where present, those centred at wavenumbers < 3500 cm^{-1} for garnet were attributed to molecular water (type M of Gose and Schmädicke, 2018) and were not quantified either. The integral molar absorption coefficient ε_i (1 mol^{-1} cm^{-2}) of both Bell et al. (1995), which is mineral-specific, and Libowitzky and Rossman (1997), which is spectrum-specific and based on weighted mean wavenumbers, was used as a calibrant. The following expression of the Beer–Lambert law served for the calculation of the structural hydroxyl content expressed as H_2O equivalent c (wt %):

$$c = \frac{A_{i,\text{tot}} \times 1.8}{D \times t \times \varepsilon_i}, \tag{1}$$

where $A_{i,\text{tot}}$ is the total integral absorbance (cm^{-1}), D is the mineral density (g cm^{-3}) calculated from endmember proportions of the average mineral core composition (Spengler et al., 2023), and t (cm) is the slab thickness. Due to the use of non-polarised light, $A_{i,\text{tot}}$ (i.e. part of the numerator in Eq. 1) for pyroxene and garnet was approached as being equivalent to 3 times A_i (Konzett et al., 2008b). Since the calibration of Bell et al. (1995) requires that the ε_i value (i.e. part of the denominator in Eq. 1) for garnet must be multiplied by 3 to be comparable to that of pyroxene, the factor 3 is cancelled out for the quantification of hydroxyl in garnet after Bell et al. (1995). Quantified hydroxyl contents were first averaged for the interior and the margin per grain and for the whole grain (by using all measurements per grain) and subsequently for each mineral per sample.

In order to estimate the uncertainty of the analytical precision, we have taken the following into account. The baseline correction of the spectra leads to variations in the determination of A_i of less than 3 % (1σ), as concluded from repeated analyses of a single spectrum (Table S2). The calculation of D is based on the mineral major element chemistry analysed by wavelength dispersive spectrometry (WDS), which usually has a precision of 0.5 %. t has a standard deviation of 1 %. The calibration of Bell et al. (1995) uses ε_i with a standard deviation of 4.0 %, 4.5 %, and 10 % for orthopyroxene, clinopyroxene, and garnet, respectively. It follows from the error propagation law for Eq. (1) that the uncertainty for c of the three minerals is 5.1 %, 5.5 %, and 10.5 %, respectively. However, the greatest source of error is the variation in absorption resulting from the limited number of different orientations of anisotropic grains in non-polarised light. This uncertainty is regarded to decrease, from about 25 % to 10 %, with an increasing number of grain orientations, from 2 to 10 (Qiu et al., 2018). Therefore, our hydroxyl contents of orthopyroxene and clinopyroxene after Bell et al. (1995) are estimated to have a total precision of 20 % or less when based on averages of 3 orientations or more. Uncertainties for values based on fewer orientations are higher, up to 80 % (Qiu et al., 2018). The regression of ε_i in the calibration of Libowitzky and Rossman (1997) is given with a reliability of 10 %–20 %, i.e. similar to the average from anisotropic grains in non-polarised light. It can therefore be assumed that the hydroxyl contents of garnet and pyroxene in Table 1 according to Libowitzky and Rossman (1997) have a similar, albeit slightly higher, total uncertainty than when using Bell et al. (1995).

Element maps of grains of clinopyroxene were performed using a JEOL JXA-8230 electron microprobe equipped with five spectrometers for WDS and one spectrometer for energy dispersive spectrometry at the Faculty of Geology, Geophysics and Environmental Protection, AGH University of Krakow, Poland. Operating conditions were 15 kV accelerating voltage and 100 nA beam current. The electron beam was focused to less than 1 µm. The dwell time was 100 ms, and step sizes of 0.5 and 1.0 µm were chosen for image areas of 90 µm × 90 µm and 610 µm × 520 µm, respectively.

4 Results

4.1 FTIR spectra

4.1.1 Clinopyroxene

Non-polarised infrared spectra of the diopsidic and omphacitic clinopyroxenes show absorption in two dominant bands at 3450–3471 and 3521–3538 cm^{-1} for all samples except UL-96-2, where the absorption in both bands is comparably low (Figs. 3a and 4a). Clinopyroxene from the latter sample exhibits an additional, pronounced absorption at higher wavenumbers in the range of 3618–3633 cm^{-1}, which is also observed in clinopyroxene of sample DS2217 but is weak or absent in those of the other samples. Further minor absorption at a wavenumber centred at approximately 3350 cm^{-1} applies to few samples. The absorbances of the two dominant absorption bands from selected spectra show strong variation in the whole data set, between 1 and 11 for a thickness normalised to 1 cm.
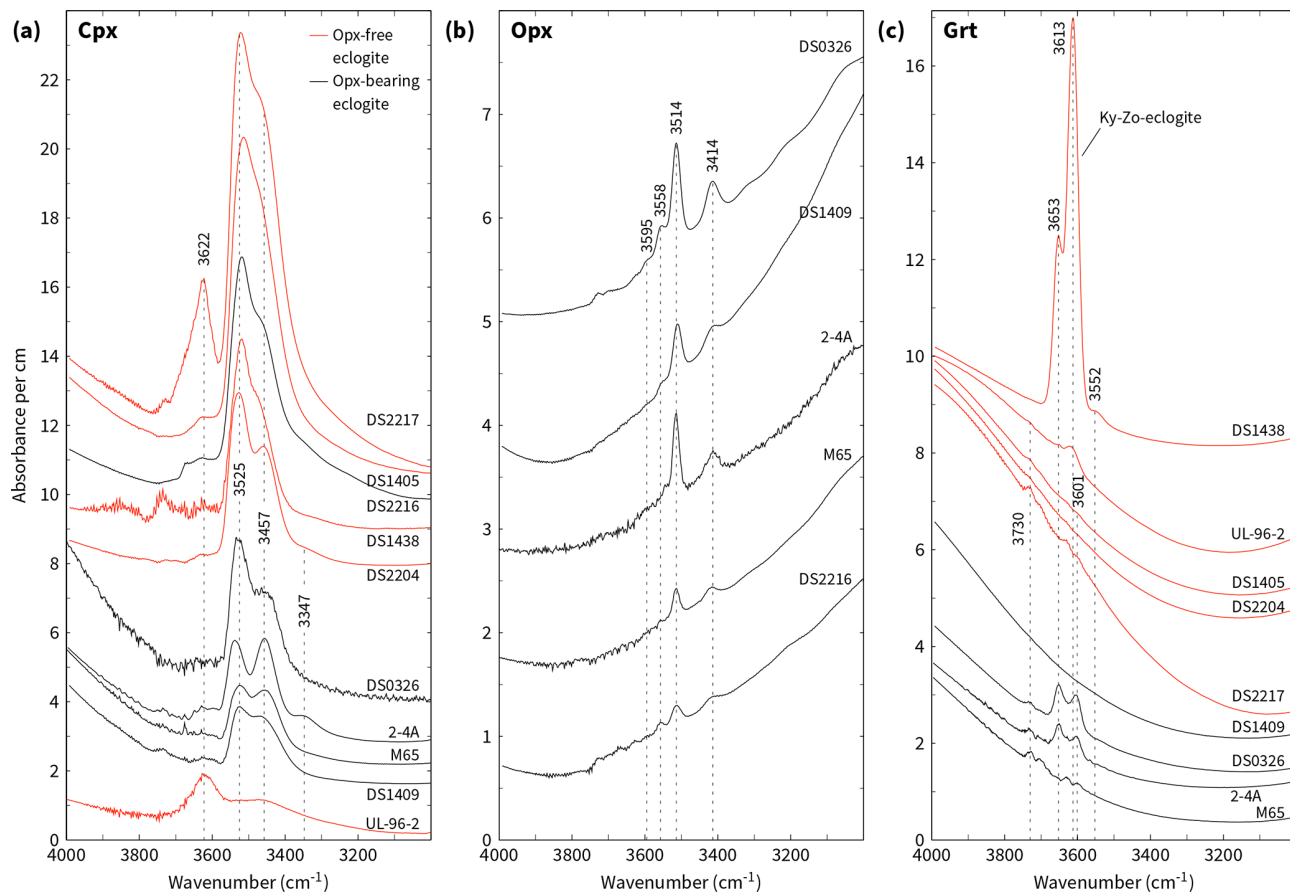
Figure 3. Representative non-polarised FTIR spectra (labels are sample numbers) in the O–H stretching frequency range normalised to 1 cm thickness and offset along the ordinate. Dashed lines indicate the position of selected peaks.
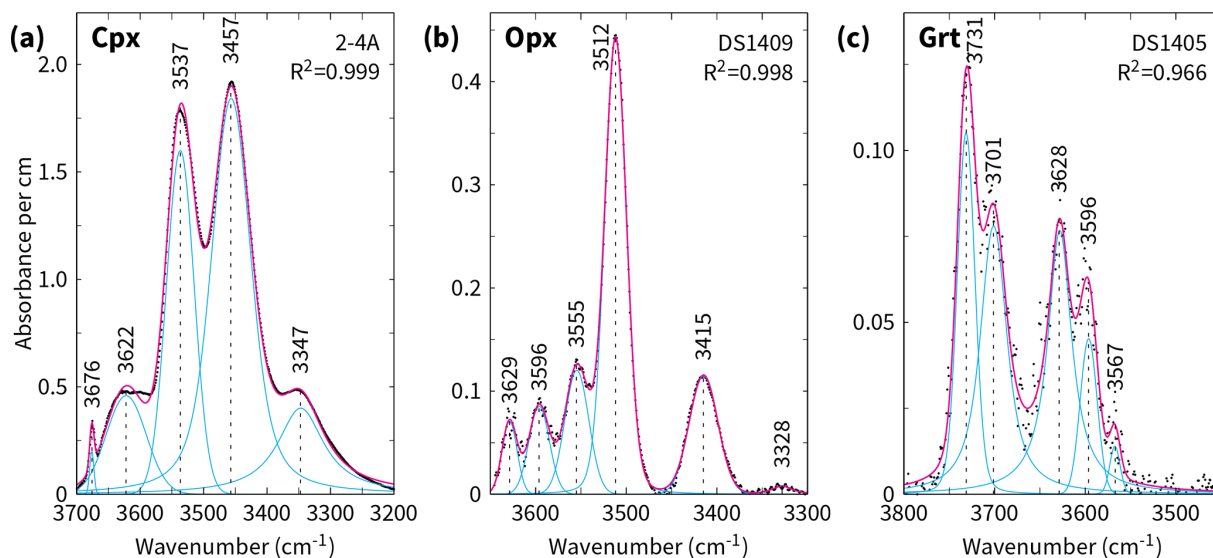
Figure 4. Baseline corrected and deconvolved FTIR spectra using Voigtian functions normalised to 1 cm thickness. Dashed lines indicate the position of selected peaks.

4.1.2 Orthopyroxene

Orthopyroxene has two large, narrow absorption peaks centred at 3415 and 3515 cm^{-1} and three to four minor peaks at higher wavenumbers centred at approximately 3555, 3565, 3595, and 3625 cm^{-1} (Figs. 3b and 4b, Table 1). Absorption at approximately 3330 cm^{-1} was rarely observed, was very small, and was therefore neglected (Fig. 4b). The intensities of the two dominant absorption bands vary considerably depending on the sample and are below 1 for a thickness normalised to 1 cm.

4.1.3 Garnet

Garnet has pronounced absorption bands with one or two peaks in each of the wavenumber ranges of 3595–3630, 3650–3660 and 3700–3735 cm^{-1} and with a smaller band centred at approximately 3560 cm^{-1} (Figs. 3c and 4c). All OH bands of the garnets analysed show low absorbance < 1 for a thickness normalised to 1 cm. An exception is sample DS1438 from the zoisite-bearing eclogite locality (Fig. 3c). If regarded separately, then garnet has rather similar variation in absorbance for orthopyroxene-bearing and orthopyroxene-free eclogites.

4.2 Major element distribution in clinopyroxene

Element concentration maps of clinopyroxene from sample DS2217 show that the core of the host grain between the monomineralic lamellae of albite is depleted in Al, Fe, and Na compared to the grain periphery (Fig. 5b–d). There, these elements occur spatially concentrated, showing thin straight lines parallel to one of the cleavage plane directions of the host grain, which coincides with one of the albite lamellae directions and the orientation of very thin lamellar inclusions between grain rims and grain cores (Fig. 5a; for higher magnification photos, the reader is referred to the previous study by Spengler et al., 2023, Fig. 5e and f). These tiny inclusions between the grain rims and cores of the clinopyroxene appear to occur only in sample DS2217. They were not observed by optical methods in any other sample in the series and were not described in the previous study.

Clinopyroxene, which hosts bimineralic lamellae of quartz and pargasite, has element concentrations around these inclusions that are depleted in Al content and enriched in Ca content; an example of this is sample M65 (Fig. S2).

4.3 Band assignment and hydroxyl content

As outlined in Sect. 3, we calculated the hydroxyl content of the NAMs with two independent calibrations: Bell et al. (1995) and Libowitzky and Rossman (1997). The hydroxyl contents determined with the calibration of Libowitzky and Rossman (1997) are 45 ± 2 % and 42 ± 4 % lower for clinopyroxene and garnet, respectively, than those of Bell et al. (1995) and 30 ± 5 % higher for orthopyroxene. The results of both calibrations are reported in Table 1, but, in order to avoid confusion, in the following, we refer only to the values determined using the absorption coefficient of Bell et al. (1995).

4.3.1 Clinopyroxene

The position of four absorption bands in clinopyroxene, centred at (1) ~ 3350 cm^{-1}, (2) 3450–3471 cm^{-1}, (3) 3521–3538 cm^{-1}, and (4) 3618–3633 cm^{-1}, is similar to that in synthetic and natural clinopyroxene with diopsidic, omphacitic, and augitic mineral chemistry reported in earlier studies (Skogby et al., 1990; Peslier et al., 2002; Koch-Müller et al., 2004; Yang et al., 2010; Gose and Schmädicke, 2022; Aulbach et al., 2023). There is agreement among them that bands (2) and (3) result from the vibration of structural hydroxyl. Band (4) was shown, on the one hand, to be related to clinopyroxene from a variety of occurrences and different chemistries, including those of aegirine and omphacite (Skogby et al., 1990, 2016), and it can form the major absorption band in lherzolitic and wehrlitic clinopyroxenes from the Pannonian Basin (Patkó et al., 2019); on the other hand, it was also shown to be associated with tiny sheet silicate inclusions occurring in eclogite xenoliths of the Siberian subcontinental lithospheric mantle (Koch-Müller et al., 2004). Given that band (4) in the current data set is dominantly minor (Fig. 3a) and strongest in sample DS2217, which has optical and mineral chemical evidence for the presence of minute lamellar inclusions (Fig. 5), band (4) in this study was assigned to sheet silicate inclusions and was therefore excluded from the quantification of structural hydroxyl.

The absorption band centred at approximately 3350 cm^{-1} may be related to structural hydroxyl or molecular water (see discussion in Gose and Schmädicke, 2022). This band has a low intensity in our data set (Fig. 4a), does not occur in all spectra (Table 1), and was included in the quantification of hydroxyl for simplicity.

The total average structural hydroxyl content of clinopyroxene in the sample set (Table 1), calculated from bands (1–3), has the range 58–711 $\mu g\,g^{-1}$ H_2O equivalent using the calibration of Bell et al. (1995). If one distinguishes between the outermost 200 μm of a grain (rim) and the grain interior (core), then the ranges for rim and core are, respectively, 119–711 and 40–539 $\mu g\,g^{-1}$.

4.3.2 Orthopyroxene

The six absorption bands in orthopyroxene, (1) 3411–3421 cm^{-1}, (2) 3511–3515 cm^{-1}, (3) 3546–3558 cm^{-1}, (4) 3565–3569 cm^{-1}, (5) 3591–3597 cm^{-1}, and (6) 3611–3629 cm^{-1}, were recognised to characterise a variety of igneous, metamorphic, and synthetic orthopyroxenes and were ascribed to intrinsic hydroxyl (Beran and Zemann, 1986; Stalder, 2004; Patkó et al., 2019; Tollan and Hermann, 2019). Absorption bands with wavenumbers between 3450

and 3630 cm^{-1} were shown to correlate with trivalent Al, Cr, and Fe in the crystal lattice (Stalder, 2004).

The integrated absorbances of bands (1–6) yielded an average structural hydroxyl content in orthopyroxene in the range of 4–17 µg g^{-1} H$_2$O equivalent. The range for grain rims is 4–15 µg g^{-1}, and that for the grain cores is slightly higher at 5–18 µg g^{-1}. Both sample-specific individual analyses (Fig. 6b) and average values (Table 1) show that the rims systematically have a lower hydroxyl content than the cores. These intracrystalline hydroxyl concentration differences do not overlap within the analytical uncertainty when analysed on a single grain (Fig. S3).

4.3.3 Garnet

The positions of the seven absorption bands in WGR eclogite garnet, (1) 3541–3573 cm^{-1}, (2) 3596–3615 cm^{-1}, (3) 3626–3642 cm^{-1}, (4) 3650–3659 cm^{-1}, (5) 3668–3694 cm^{-1}, (6) 3698–3708 cm^{-1}, and (7) 3721–3734 cm^{-1}, were previously recognised in other metamorphic and synthetic garnets and were dominantly assigned to structural hydroxyl. For example, absorption at wavenumbers within band (1) were described from Auerbach grossular (Rossman and Aines, 1991) and natural solid solutions of pyrope–almandine (Maldener et al., 2003) and almandine–grossular–pyrope (Reynes et al., 2023). Band (2) is within the range of "type II" of garnet from Erzgebirge and Fichtelgebirge eclogite, pyroxenite, and peridotite and Alpe Arami peridotite (Gose and Schmädicke, 2018; Schmädicke and Gose, 2019); characterises natural and synthetic grossular–hydrogrossular garnet (Rossman and Aines, 1991) and synthetic pyrope (Ackermann et al., 1983); and was assigned to the hydrogarnet substitution. Band (3) covers peaks ascribed to structural hydroxyl in synthetic pyrope (Geiger et al., 1991; Mookherjee and Karato, 2010). Band (4) is within the range of "type I" of Erzgebirge eclogite garnet (Gose and Schmädicke, 2018) and denotes Roberts Victor eclogite garnet (Schmädicke et al., 2015) and synthetic pyrope with reference to the hydrogarnet substitution (Geiger et al., 1991). Wavenumbers within band (5) were documented from synthetic hydrothermally grown grossular (Geiger and Armbruster, 1997); natural grossulars of gem quality (Aines and Rossman, 1984a; Maldener et al., 2003; Reynes et al., 2018) before and after annealing at 1000 °C (Zhang et al., 2022); pegmatitic grossular (Gadas et al., 2013); and megacryst pyropes from the Colorado Plateau, Wesselton kimberlite, Monastery kimberlite, and a Cr-pyrope xenocryst from the Weltevreden kimberlite (Aines and Rossman, 1984a, b; Bell and Rossman, 1992), which support a relationship with intrinsic hydroxyl over an assignment to the presence of tiny inclusions of hydrous Mg-rich layer silicates of the serpentinite group (Geiger and Rossman, 2020). Absorption within bands (6) and (7) is reported from almandine–grossular–pyrope solid-solution garnet from Dabieshan Bixiling eclogite (Xia et al., 2005; BXL15-1-2), Tibetan Sumdo eclogite (Gou et al., 2020; Y-4-

1.7), and Cima di Gagnone eclogite (Schmädicke and Gose, 2020; CG6(1)-grt4) and was considered by those authors to be unrelated to intrinsic hydroxyl or to be indicative of secondary amphibole. On the other hand, band (6) occurs in Quebec hydrogrossular, whose intrinsic hydroxyl was constrained by mineral chemistry to occupy other structural sites in garnet than those of the hydrogarnet substitution (Birkett and Trzcienski, 1984). To address this ambiguity, the hydroxyl content of WGR eclogite garnet was quantified with and without integral absorbances of bands (6) and (7).

The integral absorbances of the bands (1–5) of all garnets in this study revealed hydroxyl contents varying in the range of 2 orders of magnitude, 4–302 µg g^{-1} H$_2$O equivalents. However, when excluding the sample from the zoisite-bearing eclogite (DS1438), the range shrinks to 4–27 µg g^{-1}. Average values for rim and core areas of grains from sample DS1438 are 285 and 309 µg g^{-1}, respectively, and vary for grains of the other samples with 5–30 and 2–26 µg g^{-1}, respectively.

The integral absorbances of all bands (1–7) give hydroxyl values with a similar range of 8–306 µg g^{-1}, which shrinks to 8–38 µg g^{-1} when DS1438 garnet is excluded. Average values for rim and core areas of DS1438 garnet are 290 and 313 µg g^{-1} and vary for grains of the other samples at 7–38 and 6–27 µg g^{-1}, respectively.

5 Discussion

5.1 Variation in quantified hydroxyl

The approach of treating absorption bands (6) and (7) in garnet separately for the quantification of hydroxyl shows that the difference between minimum and maximum estimates, by using bands (1–5) and (1–7), respectively, for a given calibration does not exceed 17 µg g^{-1} and is on average 6 ± 4 µg g^{-1} (Table 1). This rather small difference particularly affects the garnet grains with the lowest hydroxyl content but is unlikely to be relevant for the interpretation of the data set. For reasons of simplicity, the following discussion will refer to the minimum estimates for hydroxyl in garnet based on the integral absorbances of bands (1–5).

Individual infrared spectra show that the structural hydroxyl content in grain rims and cores varies for a particular sample and mineral phase (Fig. 6). This variation includes differences in absorbance resulting from different orientations of anisotropic grains in non-polarised light. Therefore, the average values obtained from 2–5 grains separately for rims and cores (Table 1) likely have an uncertainty of 25 % or less (Qiu et al., 2018), which causes many of these average values to overlap within uncertainty. However, sample-specific rim / core ratios of these average hydroxyl contents are systematically below unity for orthopyroxene (Fig. 7), suggesting that orthopyroxene rims experienced late hydroxyl loss. The ratios for clinopyroxene range from unity
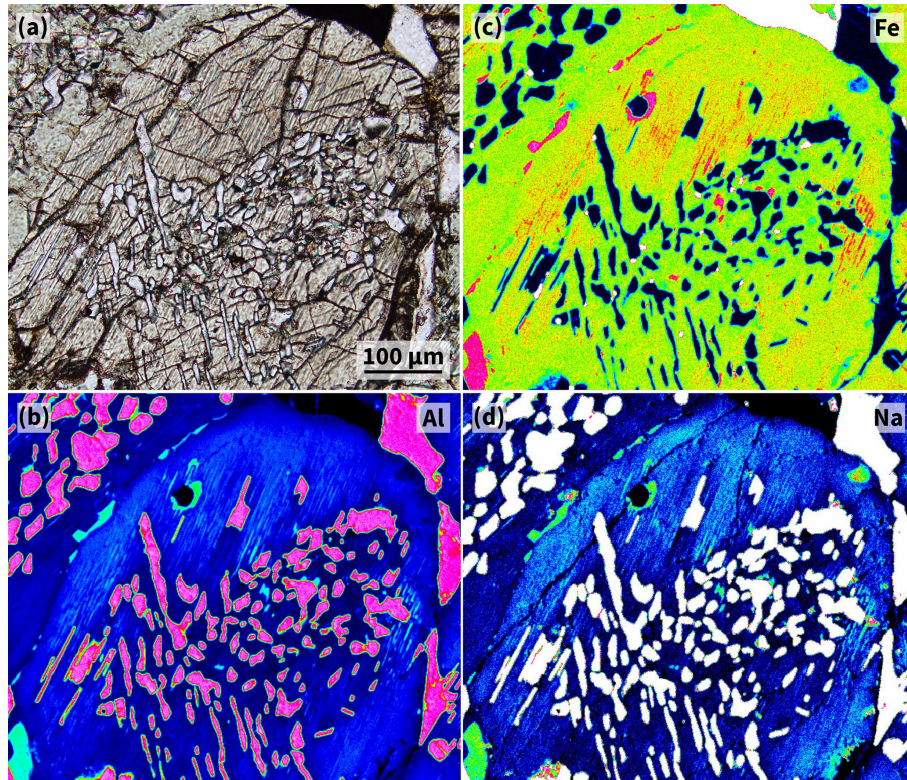
Figure 5. Oriented inclusions in Cpx from Karmannsvågen eclogite DS2217. **(a)** Photomicrograph that shows a cross-section surface of a Cpx grain (grey) with oriented lamellae and blebs of Ab several µm in width (bright) in the host crystal core and lamellae of another mineral phase with sub-µm width (slightly brownish) concentrated in between the core and rim of the host Cpx grain (plane-polarised light). **(b–d)** Compositional maps of the area shown in panel **(a)** for Al, Fe, and Na (false-colour images, element concentration increases along the colour changes black–blue–green–red–white).
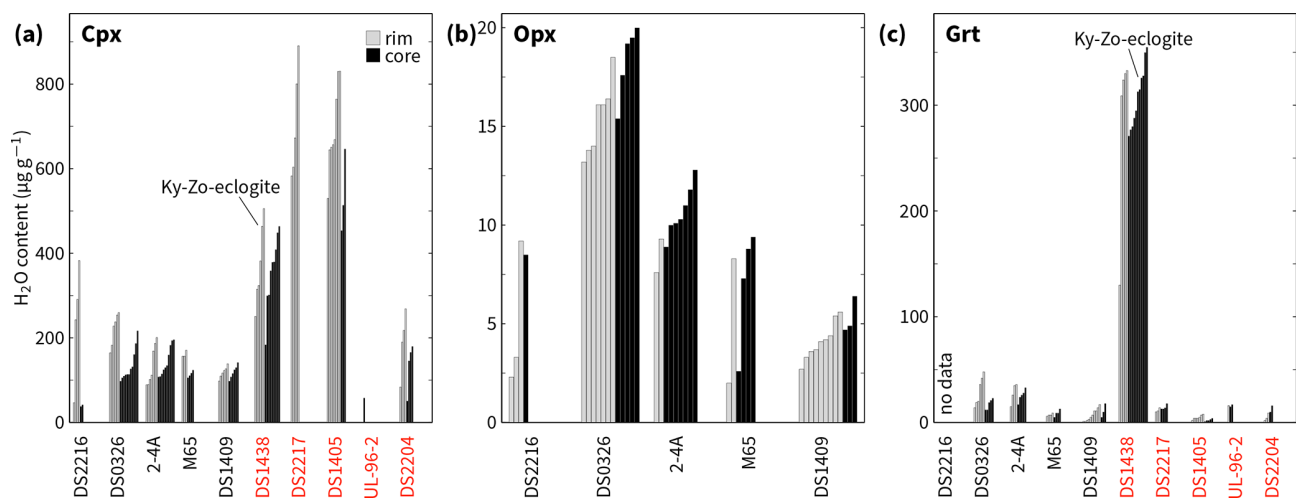
Figure 6. Structural hydroxyl contents expressed in H_2O equivalents in the grain interior (core) and outermost 200 µm (rim) quantified using individual FTIR spectra of **(a)** Cpx, **(b)** Opx, and **(c)** Grt using absorption bands (1–5) and the calibration of Bell et al. (1995). Numbers refer to sample numbers (black is Opx-bearing eclogite; red is Opx-free eclogite).
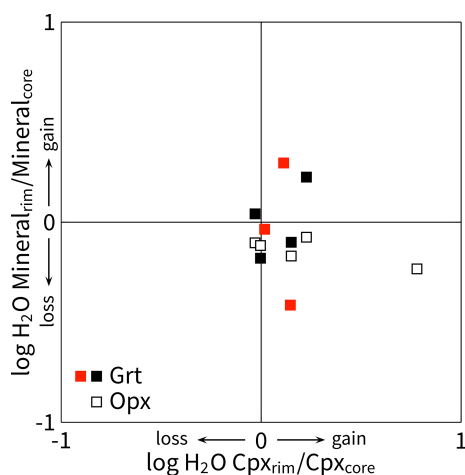
Figure 7. Bivariate plot that shows ratios calculated from rim and core average H_2O contents in NAMs given in Table 1 (red symbols show Opx-free eclogite; other symbols show Opx-bearing eclogite), using the calibration of Bell et al. (1995), and the integrated absorbance of bands (1–5) for Grt. Logarithmic values above 0 (ratios above unity) indicate that the rims contain more H_2O than the cores and vice versa.

upwards, which is consistent with the uptake of hydroxyl at the grain rims in some samples. The intragranular distribution of hydroxyl in individual grains of orthopyroxene and clinopyroxene demonstrates that the difference between core and rim contents is beyond analytical uncertainty (Figs. S3 and S4). The ratios for garnet cluster around unity, indicating indifferent behaviour. The late hydroxyl loss in orthopyroxene should be considered when interpreting the water content of this mineral from highly retrograde samples.

The hydroxyl contents determined with the calibrations of Libowitzky and Rossman (1997) and Bell et al. (1995) differ significantly. Both calibrations are based on different approaches. While the former uses wavenumber-dependent molar absorption coefficients, the latter calibration relies on mineral-specific counterparts. In the case of clinopyroxene, the absorption band at approximately $3350\,cm^{-1}$ observed in most of the WGR samples (Table 1) is absent in the augitic clinopyroxene used in the calibration of Bell et al. (1995). Besides, the quantification after Libowitzky and Rossman (1997) has been shown to be in good agreement with the ε_i of Koch-Müller et al. (2007), whose structural H_2O content was determined by secondary ion mass spectrometry, and to be more generally applicable to clinopyroxene (Weis et al., 2018). These aspects suggest that the hydroxyl content in the analysed clinopyroxene is more likely in the range of 31–$384\,\mu g\,g^{-1}$. Similar arguments could be made for the hydroxyl contents quantified for orthopyroxene and garnet. For example, the analysed orthopyroxene shows no absorption at the wavenumbers 3060 and $3300\,cm^{-1}$, which were used in the calibration of Bell et al. (1995), which in turn shows no absorption at about $3625\,cm^{-1}$. All garnet absorption

wavenumbers used in the calibration (3512 and $3571\,cm^{-1}$) barely agree in number and position with those observed in this study. For this reason, more weight may be given to hydroxyl contents quantified using the spectrum-specific approach, and their mineral-specific counterparts may be regarded as maximum estimates. However, since the two estimates differ by less than 0.5 orders of magnitude and therefore are not expected to have any influence on the interpretation of the data set, and for comparison purposes, the values from Bell et al. (1995) were used in the diagrams.

5.2 Differences in hydroxyl content during peak metamorphism

Evidence for UHP metamorphism was obtained earlier for all studied eclogite bodies, either by the current mineral chemistry applied to geothermobarometers, index mineral inclusions, reconstructed mineral chemistries from mineral microstructures, multi-equilibrium thermodynamic calculations, or a combination of the above methods (Terry et al., 2000; Carswell et al., 2003; Quas-Cohen, 2014; Spengler et al., 2023). There are two lines of evidence for differences in hydroxyl content during this UHP metamorphism. One relates to sample DS1438, whose garnet hydroxyl content is 2 orders of magnitude higher than that of garnet from any other sample (Fig. 6c). Since this is the only sample from an outcrop studied whose peak metamorphic mineral assemblage contains hydrous minerals, zoisite, and phengite (Terry et al., 2000; Liu and Massonne, 2022), the high structural hydroxyl content in its garnet is most likely related to the more hydrous conditions for the whole rock during peak metamorphism. Possible hydroxyl sources may include an inherited (pre-UHP) hydroxyl-rich precursor whole-rock chemistry or local fluids during UHP metamorphism. The hydroxyl concentration ratio between clinopyroxene and garnet in this sample is close to unity (1.2), lower than in any of the studied samples (3.5–81.8) but similar to that of zoisite-bearing mantle eclogite (1.5–2.0; Radu et al., 2022; Fig. 8).

The hydroxyl content of clinopyroxene provides the other indication. All eclogite samples with evidence for equilibration at UHP by orthopyroxene barometry, i.e. by the current mineral chemistry in addition to mineral microstructures (DS0326, 2-4A, M65, DS1409), have cores of clinopyroxene with relatively uniform hydroxyl content (114–$146\,\mu g\,g^{-1}$; Table 1). All other samples that have evidence for UHP metamorphism only by mineral microstructures but not the current mineral chemistry show large variation across all such samples (40–$539\,\mu g\,g^{-1}$). In addition, the highest hydroxyl content does not occur in clinopyroxene of the zoisite-bearing sample (Fig. 6a). This suggests that the post-peak metamorphic evolution of eclogite modified the hydroxyl content of the minerals.

Importantly, the eclogite with hydrous garnet (sample DS1438) and the orthopyroxene-bearing eclogites with anhydrous garnet (2-4A, DS0326, DS1409, M65) share oriented
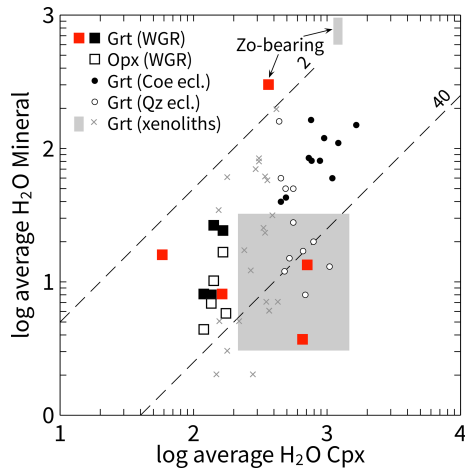
Figure 8. Bivariate plot that shows average H_2O contents in NAMs of WGR eclogite (red squares: Opx-free eclogite; other squares: Opx-bearing eclogite) using the calibration of Bell et al. (1995). Circles refer to eclogite from the Erzgebirge, Fichtelgebirge, and Kokchetav massif (Katayama et al., 2006; Gose and Schmädicke, 2018). The crosses and shaded fields are from eclogite xenoliths from the Siberian, Slave, Kaapvaal, and West African cratons, with the large field referring to the range reported from metasomatised and pristine (Type I and Type II, respectively) Roberts Victor eclogite (Bell and Rossman, 1992; Huang et al., 2014; Radu et al., 2022; Aulbach et al., 2023, 2024). Dashed lines show $D_{H_2O}^{Cpx/Grt}$ ratios that subdivide the WGR data set. The upper line (labelled 2) coincides with linearly fitted Cpx/Opx H_2O concentration ratios in global peridotite xenoliths (Demouchy and Bolfan-Casanova, 2016). The lower line (40) separates the samples secondarily enriched during retrogression.

mineral inclusions of pargasite + quartz in clinopyroxene. This indicates that the oriented mineral microstructure was formed after UHP metamorphism regardless of the presence or absence of a hydrous mineral (i.e. differences in hydrous conditions) during UHP metamorphism. The fact that the remaining bimineralic eclogite samples (DS1405, DS2204, DS2217, UL-96-2) have oriented inclusions without pargasite in clinopyroxene cores, but have clinopyroxene with the lowest and highest hydroxyl contents in the entire sample suite (Fig. 8), suggests that the processes that formed the extreme mineral hydroxyl contents and the pargasite lamellae are different (i.e. decoupled from each other). It should be noted that the major mineral element chemistry of garnet from all samples (Table S3) obtained from Spengler et al. (2023) shows little to no correlation with the hydroxyl content of clinopyroxene (Fig. S5). Likewise, the hydroxyl content of orthopyroxene is either the lowest of the three major minerals or similar to that of garnet (Fig. 9). Apparently, the presence or absence of orthopyroxene in the mineral assemblage also had no significant influence on the hydroxyl content or the hydroxyl distribution between the other two major minerals.
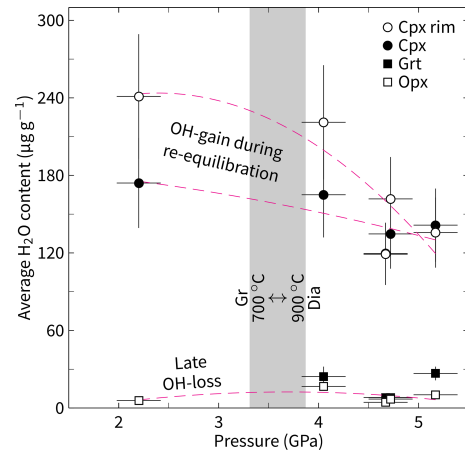
Figure 9. Average H_2O content of NAMs in WGR Opx-bearing eclogite using the calibration of Bell et al. (1995) versus metamorphic pressure calculated from the mineral chemistry of Opx and Grt given in Table 1. Uncertainties shown for H_2O refer to 20 % of the calibration used, and uncertainties shown for pressure refer to 1σ of the calibration used. The data for Cpx and Opx were fitted to a second-order polynomial (dashed lines). The Gr/Dia phase transition is shown for the temperature range 700–900 °C (grey field; Day, 2012). Note that all H_2O contents in Cpx can only represent those of the host mineral after the formation of the oriented inclusions of Qz + Prg, which are not stable during the residence of Cpx in the stability field of Dia. Thus, the proposed hydroxyl gain after the initial decompression caused an intracrystalline hydroxyl gradient that occurred after the formation of the oriented inclusions.

5.3 Post-peak metamorphic hydroxyl

The Al content in orthopyroxene, which shares a mineral paragenesis with garnet, is known to sensitively record metamorphic pressures and is therefore often used as a geobarometer. The combination of such pressure estimates with the total average structural hydroxyl content of clinopyroxene, i.e. the major host for water in eclogite in the absence of hydrous minerals, shows an inverse correlation with individual values that largely overlap in analytical uncertainty (Fig. 9). The rather large uncertainty results from the low statistics on anisotropic pyroxene. However, when the rim average hydroxyl content of clinopyroxene is used, the inverse correlation is more pronounced and the increase in hydroxyl content exceeds possible orientation effects (Fig. 9). This correlation indicates that decompression led to the incorporation of hydroxyl into clinopyroxene. The increase in structural hydroxyl content observed within individual grains from the clinoypyroxene core to the rim regions, in addition to the overall averages, indicates (i) a reliable intracrystalline difference in hydroxyl content beyond analytical uncertainty, which (ii) affects pre-existing grains after the formation of a unique mineral inclusion microstructure (Fig. S4).

Since all samples are decompressed (i.e. collected from the surface), the cause of the correlation shown in Fig. 9 is likely

not the pressure change itself but rather the mineral–chemical response to decompression (i.e. re-equilibration) that allowed clinopyroxene to incorporate additional hydroxyl. An inverse correlation between the jadeite component and the total structural hydroxyl content in clinopyroxene supports this assumption (Fig. S5b). Orthopyroxene tends to show a similar inverse relationship in the metamorphic pressure range of 4.0–5.5 GPa, which is consistent with the experimentally demonstrated dependence of the amount of structural hydroxyl on the Al content (Stalder, 2004). An exception is the strongly retrogressed sample DS2216, which shows a lower orthopyroxene hydroxyl content than expected. This low content could be related to late hydrogen loss, which is particularly plausible given the fractured nature of the crystals, as this allows diffusion to also efficiently affect the crystal core regions (cf. Sect. 5.1 and Fig. 8c in the preceding study).

Although the orthopyroxene-free eclogites have clinopyroxene with a large variation in hydroxyl content (Fig. 6a), the samples (with and without orthopyroxene) with the highest abundances in clinopyroxene (DS2216 and DS2217, respectively) are only a few hundred metres apart (Fig. 1). This suggests that the structural hydroxyl variation in orthopyroxene-free eclogite is in part also related to different degrees of retrogression.

The inverse correlation between structural hydroxyl in clinopyroxene and quantified pressure (Fig. 9) indicates that the retrogression after UHP was related to the availability of water or fluids. The same conclusion can be drawn independently from the hydroxyl content in individual crystals of clinopyroxene, which increases from the grain cores to the rims; this gradient overprints a pre-existing decompression mineral microstructure (Fig. S4). The close proximity of chemically distinct eclogites with the highest structural hydroxyl content in clinopyroxene suggests that the main pathways for the fluids may have been the foliation planes. A rough structural extrapolation of eclogite exposure with the highest structural hydroxyl content in clinopyroxene (or degree of retrogression; samples DS1405, DS2216, DS2217) could indicate two corridors between the coast and the hinterland in which efficient retrogression occurred (Fig. 1). More samples would have to be analysed to test this hypothesis. Nevertheless, the presumed corridors are situated in between two formerly separated UHP areas (Root et al., 2005; Hacker et al., 2010) and may explain why evidence for UHP metamorphic conditions in eclogite exposed in this area was difficult to detect for a long time.

5.4 Lamellae formation in clinopyroxene

The source of hydroxyl structurally bound to pargasite occurring as oriented lamellae together with quartz in clinopyroxene (Figs. 2b, S1, S2, and S4) could either be external (e.g. from an infiltrating fluid) or internal (from the water content of a precursor clinopyroxene). Several arguments are against

the first variant and in favour of the second variant. First of all, an infiltrating fluid that caused the formation of pargasite in clinopyroxene within the amphibole stability field would be expected to have simultaneously infiltrated associated orthopyroxene crystals. If this is true, then orthopyroxene is expected to record metamorphic conditions in the stability field of amphibole but not of diamond (Fig. 9). Furthermore, the occurrence of bimineralic inclusions in clinopyroxene is independent of the structural hydroxyl content of the host mineral, which increases with retrogression and is thus a function of retrogression (Fig. 9). Since the bimineralic inclusions occur regardless of the degree of retrogressive overprint (i.e. in peak metamorphic and retrogressed samples), their origin is unlikely to be related to the availability of external fluids. In addition, the compositional halos around the pargasite and quartz inclusions of more diopsidic, less aluminous clinopyroxene indicate that the pargasite formation resulted from the local decomposition of the jadeite component rather than an external fluid (Fig. S2). Finally, the K_2O content of the lamellar pargasite (Table S1) is close to the detection limit of the electron microprobe but should, arguably, be significantly higher if the lamellae were in contact with an infiltrating fluid due to the fluid mobility of K, as is assumed for comparable samples from the Alps (Konzett et al., 2008b).

With three exceptions (DS1438 as part of a zoisite–eclogite and DS1405 and DS2217, which contain abundant secondary plagioclase), the clinopyroxene host has up to several hundred micrograms per gram ($\mu g\,g^{-1}$) lower structural hydroxyl content than is typically found in comparable samples, e.g. coesite- and quartz-eclogite from the Erzgebirge (Gose and Schmädicke, 2018) and the Kokchetav massif (Katayama et al., 2006) and eclogite xenoliths (both metasomatised and pristine) reported from the Siberian, Slave, Kaapvaal, and West African cratons (Bell and Rossman, 1992; Huang et al., 2014; Aulbach et al., 2023, 2024; Fig. 8). This deficit in structural hydroxyl, when considered with the general deficit in molecular water, suggests that the monomineralic quartz lamellae (Fig. 2c and d) formed under comparatively dry conditions, as was apparently the case for the bimineralic lamellae of quartz + pargasite (Fig. 2a and b). Reintegration of hydroxyl currently bound in lamellar pargasite into the clinopyroxene precursor chemistry would increase its structural hydroxyl by about $200\,\mu g\,g^{-1}$ per percent lamellar volume. The volume fraction of lamellar pargasite was not quantified, but backscattered electron images suggest only a few percent (Figure S1b). If combined with the low hydroxyl content of the host (119–364 $\mu g\,g^{-1}$ or less; Table 1), then up to several volume percent of pargasite could have theoretically exsolved from a precursor clinopyroxene, since clinopyroxene is capable of accommodating up to more than $2000\,\mu g\,g^{-1}$ of structural hydroxyl (Katayama and Nakashima, 2003). Fluid-mediated metasomatism, on the other hand, has been shown to form amphibole lamellae in clinopyroxene and orthopyroxene in the absence of quartz lamellae (Liptai et al., 2024). Such lamellae have not been

previously reported from the samples studied but appear to occur as parallel submicrometer-sized inclusions in clinopyroxene in sample DS2217, as indicated by a strong absorption peak at 3622 cm^{-1} (Fig. 3a; Koch-Müller et al., 2004) and the spatial concentration of Na and Al typical for amphibole and layered silicates (Fig. 5). The size (thickness), mineralogy (close spatial association with quartz lamellae), and occurrence (presence in clinopyroxene but absence in orthopyroxene) of the pargasite lamellae in samples of this study differ from the microstructure of the amphibole lamellae in the samples thought to have formed by metasomatism reported by Liptai et al. (2024) and provide little support for the assumption that the bimineralic lamellae formed by a similar process.

UHP eclogites of the Kokchetav massif show that hydroxyl absorption in clinopyroxene increases with the vacancy concentration in the pyroxene structure (i.e. the Ca-Eskola component; Katayama and Nakashima, 2003). This relationship has been confirmed experimentally (Bromiley and Keppler, 2004), suggests that samples rich in exsolved quartz lamellae may also be rich in pargasite lamellae, and is consistent with a cogenetic origin of the observed bimineralic lamellar inclusions.

Finally, the distribution of structural hydroxyl between clinopyroxene and garnet, $D^{\text{Cpx/Grt}} = c_{\text{H}_2\text{O}}^{\text{Cpx}} / c_{\text{H}_2\text{O}}^{\text{Grt}}$, is greater than 40 for the most overprinted samples (i.e. those with the highest hydroxyl content in clinopyroxene: DS1405, DS2217) and significantly less than 40 for all others (Fig. 8). This systematic is consistent with experimental data showing an opposite pressure dependence of the hydrogen content in both mineral phases (Aubaud et al., 2008, and references therein). By implication, the oriented mono- and bimineralic lamellae in the eclogitic clinopyroxene formed at high pressure and before the retrogressive overprinting that caused an increase in structural hydroxyl in clinopyroxene (Fig. 9). The source of the hydrous fluid is unconstrained, but the infiltration of fluids can explain the crystallisation of hydrous phases such as the matrix biotite, which is a source of rheological weakening and thus strain partitioning. Such areas of increased deformation of gneiss have recently been shown to be more effective in retrogressive overprinting of enclosed UHP eclogite (Shulaker et al., 2024).

6 Conclusions

In this study on the structural hydroxyl content in clinopyroxene, orthopyroxene, and garnet of WGR eclogite, we come to the following conclusions:

a. The hydroxyl content of the NAMs is low, depends in the case of garnet on the peak metamorphic mineral assemblage, and shows no systematics with the occurrence of different types of lamellar inclusions in clinopyroxene.

b. Bimineralic lamellar inclusions in clinopyroxene are formed in situ by dehydration of the host mineral during decompression in the amphibole stability field rather than by an intruding hydrous component, which would presumably have obscured mineral chemical evidence of preceding metamorphism in the stability field of diamond.

c. An inverse correlation of structural hydroxyl in clinopyroxene containing bimineralic lamellae with the metamorphic pressure preserved in the associated orthopyroxene suggests a retrogressive overprint that is independent of lamellae formation. This retrogressive overprint in UHP eclogite appears to be most intense between previously recognised UHP areas.

References

Ackermann, L., Cemič, L., and Langer, K.: Hydrogarnet substitution in pyrope: a possible location for "water" in the mantle, Earth Planet. Sc. Lett., 62, 208–214, https://doi.org/10.1016/0012-821X(83)90084-5, 1983.

Aines, R. D. and Rossman, G. R.: The hydrous component in garnets: pyralspite, Am. Mineral., 69, 1116–1126, 1984a.

Aines, R. D. and Rossman, G. R.: Water content of mantle garnets, Geology, 12, 720–723, https://doi.org/10.1130/0091-7613(1984)12<720:WCOMG>2.0.CO;2, 1984b.

Anderson, E. D. and Moecher, D. P.: Omphacite breakdown reactions and relation to eclogite exhumation rates, Contrib. Mineral. Petr., 154, 253–277, https://doi.org/10.1007/s00410-007-0192-x, 2007.

Aubaud, C., Hirschmann, M. M., Withers, A. C., and Hervig, R. L.: Hydrogen partitioning between melt, clinopyroxene, and garnet at 3 GPa in a hydrous MORB with 6 wt. % H_2O, Contrib. Mineral. Petr., 156, 607–625, https://doi.org/10.1007/s00410-008-0304-2, 2008.

Aulbach, S., Stalder, R., Massuyeau, M., Stern, R. A., Ionov, D. A., and Korsakov, A. V.: Water in omphacite and garnet from pristine xenolithic eclogite: $T - X - fO_2$ controls, retentivity, and implications for electrical conductivity and deep H_2O recycling, Geochem. Geophy. Geosy., 24, e2023GC011170, https://doi.org/10.1029/2023GC011170, 2023.

Aulbach, S., Gies, N. B., Linckens, J., Stalder, R., and Viljoen, F.: Inhibited hydrogen uptake in metasomatised cratonic eclogite, Contrib. Mineral. Petr., 179, 77, https://doi.org/10.1007/s00410-024-02157-6, 2024.

Bakun-Czubarow, N.: Quartz pseudomorphs after coesite and quartz exsolutions in eclogitic ompjacites of the Złote Mountains in the Sudetes (SW Poland), Archiwum mineralogiczne, 48, 3–25, 1992.

Bell, D. R. and Rossman, G. R.: The distribution of hydroxyl in garnets from the subcontinental mantle of southern Africa, Contrib. Mineral. Petr., 111, 161–178, 1992.

Bell, D. R., Ihinger, P. D., and Rossman, G. R.: Quantitative analysis of trace OH in garnet and pyroxenes, Am. Mineral., 80, 465–474, https://doi.org/10.2138/am-1995-5-608, 1995.

Beran, A. and Zemann, J.: The pleochroism of a gem-quality enstatite in the region of the OH stretching frequency, with a stereochemical interpretation, Tscher. Miner. Petrog., 35, 19–25, https://doi.org/10.1007/BF01081915, 1986.

Birkett, T. C. and Trzcienski Jr, W. E.: Hydrogarnet: multi-site hydrogen occupancy in the garnet structure, Can. Mineral., 22, 675–680, 1984.

Bromiley, G. D. and Keppler, H.: An experimental investigation of hydroxyl solubility in jadeite and Na-rich clinopyroxenes, Contrib. Mineral. Petr., 147, 189–200, https://doi.org/10.1007/s00410-003-0551-1, 2004.

Brueckner, H. K.: Sinking intrusion model for the emplacement of garnet-bearing peridotites into continent collision orogens, Geology, 26, 631–634, https://doi.org/10.1130/0091-7613(1998)026<0631:SIMFTE>2.3.CO;2, 1998.

Carswell, D. A., Harvey, M. A., and Al-Samman, A.: The petrogenesis of contrasting Fe-Ti and Mg-Cr garnet peridotite types in the high grade gneiss complex of Western Norway, B. Mineral., 106, 727–750, https://doi.org/10.3406/bulmi.1983.7696, 1983.

Carswell, D. A., Tucker, R. D., O'Brien, P. J., and Krogh, T. E.: Coesite micro-inclusions and the U/Pb age of zircons from the Hareidland Eclogite in the Western Gneiss Region of Norway, Lithos, 67, 181–190, https://doi.org/10.1016/S0024-4937(03)00014-8, 2003.

Cuthbert, S. J., Carswell, D. A., Krogh-Ravna, E. J., and Wain, A.: Eclogites and eclogites in the Western Gneiss Region, Norwegian Caledonides, Lithos, 52, 165–195, https://doi.org/10.1016/S0024-4937(99)00090-0, 2000.

Day, H. W.: A revised diamond-graphite transition curve, Am. Mineral., 97, 52–62, https://doi.org/10.2138/am.2011.3763, 2012.

Demouchy, S. and Bolfan-Casanova, N.: Distribution and transport of hydrogen in the lithospheric mantle: a review, Lithos, 240–243, 402–425, https://doi.org/10.1016/j.lithos.2015.11.012, 2016.

Dobrzhinetskaya, L. F., Eide, E. A., Larsen, R. B., Sturt, B. A., Trønnes, R. G., Smith, D. C., Taylor, W. R., and Posukhova, T. V.: Microdiamond in high-grade metamorphic rocks from the Western Gneiss region, Norway, Geology, 23, 597–600, https://doi.org/10.1130/0091-7613(1995)023<0597:MIHGMR>2.3.CO;2, 1995.

Dobrzhinetskaya, L. F., Schweinehage, R., Massonne, H.-J., and Green, H. W.: Silica precipitates in omphacite from eclogite at Alpe Arami, Switzerland: evidence of deep subduction, J. Metamorph. Geol., 20, 481–492, https://doi.org/10.1046/j.1525-1314.2002.00383.x, 2002.

Gadas, P., Novák, M., Talla, D., and Vašinová Galiová, M.: Compositional evolution of grossular garnet from leucotonalitic pegmatite at Ruda nad Moravou, Czech Republic; a complex EMPA, LA-ICP-MS, IR and CL study, Miner. Petrol., 107, 311–326, https://doi.org/10.1007/s00710-012-0232-8, 2013.

Gee, D. G., Kumpulainen, R., Roberts, D., Stephens, M. B., Thon, A., and Zachrisson, E.: Scandinavian Tectonostratigraphic Map, Sveriges Geologiska Undersökning Serie Ba, https://resource.sgu.se/dokument/publikation/ba/ba35karta/ba35-karta.pdf (last access: 28 February 2025), ISBN 91-7158-357-2, 1985.

Gee, D. G., Janák, M., Majka, J., Robinson, P., and van Roermund, H.: Subduction along and within the Baltoscandian margin during closing of the Iapetus Ocean and Baltica-Laurentia collision, Lithosphere, 5, 169–178, https://doi.org/10.1130/L220.1, 2013.

Geiger, C. A. and Armbruster, T.: $Mn_3Al_2Si_3O_{12}$ spessartine and $Ca_3Al_2Si_3O_{12}$ grossular garnet: structural dynamic and thermodynamic properties, Am. Mineral., 82, 740–747, 1997.

Geiger, C. A. and Rossman, G. R.: Micro- and nano-size hydrogarnet clusters and proton ordering in calcium silicate garnet: Part I. The quest to understand the nature of "water" in garnet continues, Am. Mineral., 105, 455–467, https://doi.org/10.2138/am-2020-7256, 2020.

Geiger, C. A., Langer, K., Bell, D. R., Rossman, G. R., and Winkler, B.: The hydroxide component in synthetic pyrope, Am. Mineral., 76, 49–59, 1991.

Gose, J. and Schmädicke, E.: Water incorporation in garnet: coesite versus quartz eclogite from Erzgebirge and Fichtelgebirge, J. Petrol., 59, 207–232, https://doi.org/10.1093/petrology/egy022, 2018.

Gose, J. and Schmädicke, E.: H$_2$O in omphacite of quartz and coesite eclogite from Erzgebirge and Fichtelgebirge, Germany, J. Metamorph. Geol., 40, 665–686, https://doi.org/10.1111/jmg.12642, 2022.

Gou, Y., Wang, Q., Li, Y., and Wirth, R.: Water content in garnet from eclogites: implications for water cycle in subduction channels, Minerals, 10, 410, https://doi.org/10.3390/min10050410, 2020.

Griffin, W. L. and Brueckner, H. K.: Caledonian Sm-Nd ages and a crustal origin for Norwegian eclogites, Nature, 285, 319–321, 1980.

Hacker, B. R., Andersen, T. B., Johnston, S., Kylander–Clark, A. R. C., Peterman, E. M., Walsh, E. O., and Young, D.: High-temperature deformation during continental-margin subduction & exhumation: the ultrahigh-pressure Western Gneiss Region of Norway, Tectonophysics, 480, 149–171, https://doi.org/10.1016/j.tecto.2009.08.012, 2010.

Huang, J.-X., Li, P., Griffin, W. L., Xia, Q.-K., Gréau, Y., Pearson, N. J., and O'Reilly, S. Y.: Water contents of Roberts Victor xenolithic eclogites: primary and metasomatic controls, Contrib. Mineral. Petr., 168, 1092, https://doi.org/10.1007/s00410-014-1092-5, 2014.

Janák, M., Froitzheim, N., Lupták, B., Vrabec, M., and Krogh Ravna, E. J.: First evidence for ultrahigh-pressure metamorphism of eclogites in Pohorje, Slovenia: Tracing deep continental subduction in the Eastern Alps, Tectonics, 23, TC5014, https://doi.org/10.1029/2004TC001641, 2004.

Janák, M., van Roermund, H., Majka, J., and Gee, D.: UHP metamorphism recorded by kyanite-bearing eclogite in the Seve Nappe Complex of northern Jämtland, Swedish Caledonides, Gondwana Res., 23, 865–879, https://doi.org/10.1016/j.gr.2012.06.012, 2013.

Katayama, I. and Nakashima, S.: Hydroxyl in clinopyroxene from the deep subducted crust: evidence for H$_2$O transport into the mantle, Am. Mineral., 88, 229–234, https://doi.org/10.2138/am-2003-0126, 2003.

Katayama, I., Parkinson, C. D., Okamoto, K., Nakajima, Y., and Maruyama, S.: Supersilicic clinopyroxene and silica exsolution in UHPM eclogite and pelitic gneiss from the Kokchetav massif, Kazakhstan, Am. Mineral., 85, 1368–1374, https://doi.org/10.2138/am-2000-1004, 2000.

Katayama, I., Nakashima, S., and Yurimoto, H.: Water content in natural eclogite and implication for water transport into the deep upper mantle, Lithos, 86, 245–259, https://doi.org/10.1016/j.lithos.2005.06.006, 2006.

Koch-Müller, M., Matsyuk, S. S., and Wirth, R.: Hydroxyl in omphacites and omphacitic clinopyroxenes of upper mantle to lower crustal origin beneath the Siberian platform, Am. Mineral., 89, 921–931, https://doi.org/10.2138/am-2004-0701, 2004.

Koch-Müller, M., Abs-Wurmbach, I., Rhede, D., Kahlenberg, V., and Matsyuk, S.: Dehydration experiments on natural omphacites: qualitative and quantitative characterization by various spectroscopic methods, Phys. Chem. Miner., 34, 663–678, https://doi.org/10.1007/s00269-007-0181-7, 2007.

Konzett, J., Frost, D. J., Proyer, A., and Ulmer, P.: The Ca-Eskola component in eclogitic clinopyroxene as a function of pressure, temperature and bulk composition: an experimental study to 15 GPa with possible implications for the formation of oriented

SiO$_2$-inclusions in omphacite, Contrib. Mineral. Petr., 155, 215–228, https://doi.org/10.1007/s00410-007-0238-0, 2008a.

Konzett, J., Libowitzky, E., Hejny, C., Miller, C., and Zanetti, A.: Oriented quartz+calcic amphibole inclusions in omphacite from the Saualpe and Pohorje Mountain eclogites, Eastern Alps–An assessment of possible formation mechanisms based on IR- and mineral chemical data and water storage in Eastern Alpine eclogites, Lithos, 106, 336–350, https://doi.org/10.1016/j.lithos.2008.09.002, 2008b.

Krill, A. G.: Tectonics of the Oppdal area, central Norway, Geol. Foren. Stock. For., 102, 523–530, https://doi.org/10.1080/11035898009454505, 1980.

Kullerud, L., Tørudbakken, B. O., and Ilebekk, S.: A compilation of radiometric age determinations from the Western Gneiss Region, south Norway, Norg. Geol. Unders. B., 406, 17–42, 1986.

Libowitzky, E. and Rossman, G. R.: An IR absorption calibration for water in minerals, Am. Mineral., 82, 1111–1115, https://doi.org/10.2138/am-1997-11-1208, 1997.

Liptai, N., Lange, T. P., Patkó, L., Aradi, L. E., Berkesi, M., Tollan, P. M. E., Padrón-Navarta, J. A., Hermann, J., Gergely, S., Szabó, C., and Kovács, I. J.: Formation of amphibole lamellae in mantle pyroxene by fluid-mediated metasomatism: a focal plane array FTIR study from the Carpathian-Pannonian region, Am. Mineral., 109, 87–102, https://doi.org/10.2138/am-2022-8662, 2024.

Liu, P. and Massonne, H.-J.: High-pressure granulite facies reequilibration and zoisite–biotite dehydration melting during decompression of an ultrahigh-pressure garnet clinopyroxenite from the island of Fjørtoft, Norway, J. Metamorph. Geol., 40, 887–918, https://doi.org/10.1111/jmg.12649, 2022.

Locock, A. J.: An Excel spreadsheet to classify chemical analyses of amphiboles following the IMA 2012 recommendations, Comput. Geosci., 62, 1–11, https://doi.org/10.1016/j.cageo.2013.09.011, 2014.

Maldener, J., Hösch, A., K.Langer, and Rauch, F.: Hydrogen in some natural garnets studied by nuclear reaction analysis and vibrational spectroscopy, Phys. Chem. Miner., 30, 337–344, https://doi.org/10.1007/s00269-003-0321-7, 2003.

Mookherjee, M. and Karato, S.-i.: Solubility of water in pyrope-rich garnet at high pressures and temperature, Geophys. Res. Lett., 37, L03310, https://doi.org/10.1029/2009GL041289, 2010.

Neri, F., Saitta, G., and Chiofalo, S.: A simple procedure to remove the interference fringes from optical spectra, J. Phys. E Sci. Instrum., 20, 894–896, https://doi.org/10.1088/0022-3735/20/7/015, 1987.

Patkó, L., Liptai, N., Kovács, I. J., Aradi, L. E., Xia, Q.-K., Ingrin, J., Mihály, J., O'Reilly, S. Y., Griffin, W. L., Wesztergom, V., and Szabó, C.: Extremely low structural hydroxyl contents in upper mantle xenoliths from the Nógrád-Gömör Volcanic Field (northern Pannonian Basin): Geodynamic implications and the role of post-eruptive re-equilibration, Chem. Geol., 507, 23–41, https://doi.org/10.1016/j.chemgeo.2018.12.017, 2019.

Peslier, A. H., Luhr, J. F., and Post, J.: Low water contents in pyroxenes from spinel-peridotites of the oxidized, sub-arc mantle wedge, Earth Planet. Sc. Lett., 201, 69–86, https://doi.org/10.1016/S0012-821X(02)00663-5, 2002.

Proyer, A., Krenn, K., and Hoinkes, G.: Oriented precipitates of quartz and amphibole in clinopyroxene of metabasites from the Greek Rhodope: a product of open system precipitation during eclogite–granulite–amphibolite transition, J. Metamorph. Geol.,

27, 639–654, https://doi.org/10.1111/j.1525-1314.2009.00844.x, 2009.

Qiu, Y., Jiang, H., Kovács, I., Xia, Q.-k., and Yang, X.: Quantitative analysis of H-species in anisotropic minerals by unpolarized infrared spectroscopy: An experimental evaluation, Am. Mineral., 103, 1761–1769, https://doi.org/10.2138/am-2018-6620, 2018.

Quas-Cohen, A. C.: Norwegian orthopyroxene eclogites: petrogenesis and implications for metasomatism and crust-mantle interactions during subduction of continental crust, PhD thesis, University of Manchester, https://research.manchester.ac.uk/en/studentTheses/norwegian-orthopyroxene-eclogites-petrogenesis-and-implications-f (last access: 28 February 2025), 2014.

Radu, I. B., Moine, B. N., Bolfan-Casanova, N., Ionov, D. A., Devidal, J. L., Deloule, E., Korsakov, A. V., Golovin, A. V., Oleinikov, O. B., and Cottin, J. Y.: Zoisite in cratonic eclogite xenoliths - Implications for water in the upper mantle, Lithos, 418–419, 106681, https://doi.org/10.1016/j.lithos.2022.106681, 2022.

Reynes, J., Jollands, M., Hermann, J., and Ireland, T.: Experimental constraints on hydrogen diffusion in garnet, Contrib. Mineral. Petr., 173, 69, https://doi.org/10.1007/s00410-018-1492-z, 2018.

Reynes, J., Hermann, J., Lanari, P., and Bovay, T.: OH incorporation and retention in eclogite-facies garnets from the Zermatt–Saas area (Switzerland) and their contribution to the deep water cycle, Eur. J. Mineral., 35, 679–701, https://doi.org/10.5194/ejm-35-679-2023, 2023.

Root, D. B., Hacker, B. R., Gans, P. B., Ducea, M. N., Eide, E. A., and Mosenfelder, J. L.: Discrete ultrahigh-pressure domains in the Western Gneiss Region, Norway: implications for formation and exhumation, J. Metamorph. Geol., 23, 45–61, https://doi.org/10.1111/j.1525-1314.2005.00561.x, 2005.

Rossman, G. R. and Aines, R. D.: The hydrous components in garnets: grossular-hydrogrossular, Am. Mineral., 76, 1153–1164, 1991.

Schmädicke, E. and Gose, J.: Low water contents in garnet of orogenic peridotite: clues for an abyssal or mantle-wedge origin?, Eur. J. Mineral., 31, 715–730, https://doi.org/10.1127/ejm/2019/0031-2880, 2019.

Schmädicke, E. and Gose, J.: Water in garnet of garnetite (metarodingite) and eclogite from the Erzgebirge and the Lepontine Alps, J. Metamorph. Geol., 38, 905–933, https://doi.org/10.1111/jmg.12554, 2020.

Schmädicke, E. and Müller, W. F.: Unusual exsolution phenomena in omphacite and partial replacement of phengite by phlogopite + kyanite in an eclogite from the Erzgebirge, Contrib. Mineral. Petr., 139, 629–642, https://doi.org/10.1007/s004100000161, 2000.

Schmädicke, E., Gose, J., Reinhardt, J., Will, T. M., and Stalder, R.: Garnet in cratonic and non-cratonic mantle and lower crustal xenoliths from southern Africa: composition, water incorporation and geodynamic constraints, Precambrian Res., 270, 285–299, https://doi.org/10.1016/j.precamres.2015.09.019, 2015.

Schönig, J., Meinhold, G., von Eynatten, H., and Lünsdorf, N. K.: Tracing ultrahigh-pressure metamorphism at the catchment scale, Sci. Rep., 8, 2931, https://doi.org/10.1038/s41598-018-21262-8, 2018.

Shatsky, V. S., Sobolev, N. V., and Stenina, N. G.: Structural peculiarities of pyroxenes from eclogites, Terra Cognita, 5, 436–437, 1985.

Shulaker, D. Z., Gordon, S. M., Hammerli, J., and DesOrmeau, J. W.: Fluid-driven mass transfer during retrograde metamorphism and exhumation of the UHP Western Gneiss Region terrane, Norway, Geochem. Geophy., Geosy., 25, e2022GC010659, https://doi.org/10.1029/2022GC010659, 2024.

Skogby, H., Bell, D. R., and Rossman, G. R.: Hydroxide in pyroxene: variations in the natural environment, Am. Mineral., 75, 764–774, 1990.

Skogby, H., Janák, M., and Broska, I.: Water incorporation in omphacite: concentrations and compositional relations in ultrahigh-pressure eclogites from Pohorje, Eastern Alps, Eur. J. Mineral., 28, 631–639, https://doi.org/10.1127/ejm/2016/0028-2533, 2016.

Smith, D. C.: Coesite in clinopyroxene in the Caledonides and its implications for geodynamics, Nature, 310, 641–644, https://doi.org/10.1038/310641a0, 1984.

Smith, D. C. and Godard, G.: A Raman spectroscopic study of diamond and disordered sp^3-carbon in the coesite-bearing Straumen Eclogite Pod, Norway, J. Metamorph. Geol., 31, 19–33, https://doi.org/10.1111/jmg.12007, 2013.

Song, S. G., Yang, J. S., Xu, Z. Q., Liou, J. G., and Shi, R. D.: Metamorphic evolution of the coesite-bearing ultrahigh-pressure terrane in the North Qaidam, Northern Tibet, NW China, J. Metamorph. Geol., 21, 631–644, https://doi.org/10.1046/j.1525-1314.2003.00469.x, 2003.

Spencer, K. J., Hacker, B. R., Kylander-Clark, A. R. C., Andersen, T. B., Cottle, J. M., Stearns, M. A., Poletti, J. E., and Seward, G. G. E.: Campaign-style titanite U–Pb dating by laser-ablation ICP: implications for crustal flow, phase transformations and titanite closure, Chem. Geol., 341, 84–101, https://doi.org/10.1016/j.chemgeo.2012.11.012, 2013.

Spengler, D., Brueckner, H. K., van Roermund, H. L. M., Drury, M. R., and Mason, P. R. D.: Long-lived, cold burial of Baltica to 200 km depth, Earth Planet. Sc. Lett., 281, 27–35, https://doi.org/10.1016/j.epsl.2009.02.001, 2009.

Spengler, D., Alifirova, T. A., and van Roermund, H. L. M.: Subcratonic and tectonic evolution of pyroxenite and eclogite with lamellar inclusions in garnet, Western Gneiss Region, Norway, J. Petrol., 62, egab008, https://doi.org/10.1093/petrology/egab008, 2021.

Spengler, D., Włodek, A., Zhong, X., Loges, A., and Cuthbert, S. J.: Retrogression of ultrahigh-pressure eclogite, Western Gneiss Region, Norway, Eur. J. Mineral., 35, 1125–1147, https://doi.org/10.5194/ejm-35-1125-2023, 2023.

Stalder, R.: Influence of Fe, Cr and Al on hydrogen incorporation in orthopyroxene, Eur. J. Mineral., 16, 703–711, https://doi.org/10.1127/0935-1221/2004/0016-0703, 2004.

Terry, M. P., Robinson, P., and Krogh Ravna, E. J.: Kyanite eclogite thermobarometry and evidence for thrusting of UHP over HP metamorphic rocks, Nordøyane, Western Gneiss Region, Norway, Am. Mineral., 85, 1637–1650, https://doi.org/10.2138/am-2000-11-1207, 2000.

Tollan, P. and Hermann, J.: Arc magmas oxidized by water dissociation and hydrogen incorporation in orthopyroxene, Nat. Geosci., 12, 667–671, https://doi.org/10.1038/s41561-019-0411-x, 2019.

Tucker, R. D., Krogh, T. E., and Råheim, A.: Proterozoic evolution and age-province boundaries in the central part of the Western Gneiss Region, Norway: results of U-Pb dating of accessory minerals from Trondheimsfjord to Geiranger, vol. Special Pa-

per 38, Geological Association of Canada, ISBN 978-0-919216-45-7, 149–173, 1990.

Tucker, R. D., Robinson, P., Solli, A., Gee, D. G., Thorsnes, T., Krogh, T. E., Nordgulen, Ø., and Bickford, M. E.: Thrusting and extension in the Scandian hinterland, Norway: new U-Pb ages and tectonostratigraphic evidence, Am. J. Sci., 304, 477–532, https://doi.org/10.2475/ajs.304.6.477, 2004.

van Roermund, H. L. M., Carswell, D. A., Drury, M. R., and Heijboer, T. C.: Microdiamonds in a megacrystic garnet websterite pod from Bardane on the island of Fjørtoft, western Norway: evidence for diamond formation in mantle rocks during deep continental subduction, Geology, 30, 959–962, https://doi.org/10.1130/0091-7613(2002)030<0959:MIAMGW>2.0.CO;2, 2002.

Vrijmoed, J. C., van Roermund, H. L. M., and Davies, G. R.: Evidence for diamond-grade ultra-high pressure metamorphism and fluid interaction in the Svartberget Fe–Ti garnet peridotite–websterite body, Western Gneiss Region, Norway, Miner. Petrol., 88, 381–405, https://doi.org/10.1007/s00710-006-0160-6, 2006.

Wain, A.: New evidence for coesite in eclogite and gneisses: defining an ultrahigh-pressure province in the Western Gneiss region of Norway, Geology, 25, 927–930, https://doi.org/10.1130/0091-7613(1997)025<0927:NEFCIE>2.3.CO;2, 1997.

Wain, A., Waters, D., Jephcoat, A., and Olijynk, H.: The high-pressure to ultrahigh-pressure eclogite transition in the Western Gneiss Region, Norway, Eur. J. Mineral., 12, 667–687, https://doi.org/10.1127/0935-1221/2000/0012-0667, 2000.

Walczak, K., Cuthbert, S., Kooijman, E., Majka, J., and Smit, M. A.: U–Pb zircon age dating of diamond-bearing gneiss from Fjørtoft reveals repeated burial of the Baltoscandian margin during the Caledonian Orogeny, Geol. Mag., 156, 1949–1964, https://doi.org/10.1017/S0016756819000268, 2019.

Walsh, E. O. and Hacker, B. R.: The fate of subducted continental margins: two-stage exhumation of the high-pressure to ultrahigh-pressure Western Gneiss Region, Norway, J. Metamorph. Geol., 22, 671–687, https://doi.org/10.1111/j.1525-1314.2004.00541.x, 2004.

Warr, L. N.: IMA–CNMNC approved mineral symbols, Mineral. Mag., 85, 291–320, https://doi.org/10.1180/mgm.2021.43, 2021.

Weis, F. A., Ros, L., Reichart, P., Skogby, H., Kristiansson, P., and Dollinger, G.: Hydrogen concentration analysis in clinopyroxene using proton–proton scattering analysis, Phys. Chem. Miner., 45, 669–678, https://doi.org/10.1007/s00269-018-0953-2, 2018.

Wojdyr, M.: Fityk: a general-purpose peak fitting program, J. Appl. Crystallogr., 43, 1126–1128, https://doi.org/10.1107/S0021889810030499, 2010.

Xia, Q.-K., Sheng, Y.-M., Yang, X.-Z., and Yu, H.-M.: Heterogeneity of water in garnets from UHP eclogites, eastern Dabieshan, China, Chem. Geol., 224, 237–246, https://doi.org/10.1016/j.chemgeo.2005.08.003, 2005.

Yang, Y., Xia, Q., Feng, M., and Zhang, P.: Temperature dependence of IR absorption of OH species in clinopyroxene, Am. Mineral., 95, 1439–1443, https://doi.org/10.2138/am.2010.3501, 2010.

Young, D. J.: Structure of the (ultra)high-pressure Western Gneiss Region, Norway: imbrication during Caledonian continental margin subduction, Geol. Soc. Am. Bull., 130, 926–940, https://doi.org/10.1130/B31764.1, 2018.

Zhang, K., Liu, H., Ionov, D. A., and Yang, X.: Effects of oxygen fugacity on hydroxyl incorporation in garnet at 1–3 GPa and 800–1000 °C and implications for water storage in the mantle, J. Geophys. Res.-Sol. Ea., 127, e2022JB023948, https://doi.org/10.1029/2022JB023948, 2022.

Zhang, L., Song, S., Liou, J. G., Ai, Y., and Li, X.: Relict coesite exsolution in omphacite from western Tianshan eclogites, China, Am. Mineral., 90, 181–186, https://doi.org/10.2138/am.2005.1587, 2005.